

Chebyshev approximation and composition of functions in matrix product states for quantum-inspired numerical analysis

Juan José Rodríguez-Aldavero,¹ Paula García-Molina,¹ Luca Tagliacozzo,¹ and Juan José García-Ripoll¹

¹*Institute of Fundamental Physics IFF-CSIC, Calle Serrano 113b, Madrid 28006, Spain*

(Dated: Jul 2024)

This work explores the representation of univariate and multivariate functions as matrix product states (MPS), also known as quantized tensor-trains (QTT). It proposes an algorithm that employs iterative Chebyshev expansions and Clenshaw evaluations to represent analytic and highly differentiable functions as MPS Chebyshev interpolants. It demonstrates rapid convergence for highly-differentiable functions, aligning with theoretical predictions, and generalizes efficiently to multidimensional scenarios. The performance of the algorithm is compared with that of tensor cross-interpolation (TCI) and multiscale interpolative constructions through a comprehensive comparative study. When function evaluation is inexpensive or when the function is not analytical, TCI is generally more efficient for function loading. However, the proposed method shows competitive performance, outperforming TCI in certain multivariate scenarios. Moreover, it shows advantageous scaling rates and generalizes to a wider range of tasks by providing a framework for function composition in MPS, which is useful for non-linear problems and many-body statistical physics.

I. INTRODUCTION

Tensor networks [1] are decompositions of tensors in networks of mutually contracted smaller tensors. On some occasions, these decompositions can result in accurate, exponentially more efficient approximations. Matrix product states (MPS), originally discovered in the study of strongly correlated quantum systems and quantum Markov chains [2, 3], are a successful example of these decompositions. MPS underlie the structure of the DMRG algorithm [4, 5], a well-known and powerful method for diagonalizing many-body Hamiltonians [6]. They were rediscovered under the name of tensor-trains (TT) [7] and quantized tensor-trains (QTT) [8] as an efficient decomposition of high-dimensional tensors, featuring approximation tools similar to DMRG. Currently, MPS stand as a platform for *quantum-inspired* numerical methods [9], with applications in Fourier analysis and interpolation [9–12], extrapolation [13], solving differential equations [14–17] and multivariate integration [18–20], among others. These methods potentially yield exponential advantages in time and memory usage over conventional numerical techniques [15, 16, 20]. Furthermore, the interpretation of tensor network formalisms as quantum circuits [21] makes them an efficient method for discovering quantum algorithms to load specific functions in quantum registers [22], thus interfacing with quantum computing applications.

A central problem in using tensor-network decompositions for numerical analysis is loading generic functions into such representations. The conventional approach is based on discretizing such functions over a multidimensional grid and using singular value decompositions (SVD). However, this method scales polynomially in time and memory with the volume of the grid, thus exponentially with its dimension, becoming susceptible to the so-called “curse of dimensionality”. There are essentially two types of methods that tackle this curse. Some

methods rely on a clever sampling of the function to gather an optimal tensor network structure. This family of methods includes multiple variations of tensor cross-interpolation (TCI) [23] and generative modeling techniques [24]. Other approaches rely on algebraic representations of the function that enable constructive approximations of the optimal tensor structure. These include methods based on polynomial interpolation [25, 26] and algorithmic constructs that map concrete algebraic representations of functions to tensor networks [19].

In this work, we propose a combination of the latter two approaches, relying on Chebyshev interpolation [27, 28] to create polynomial approximations that can be efficiently constructed as MPS, using a finite-precision non-linear algebra framework [9, 16]. This extends the algebraic circuits from Ref. [19] to more generic function representations. The resulting algorithm, heavily inspired by previous uses of quantum filters [29], provides approximations that converge exponentially fast with the circuit depth for analytic functions. Furthermore, this method not only allows us to express a generic function $f(x)$ but also to combine approximations, composing functions $f(g(x))$ for which a Chebyshev interpolant has been developed, as well as their derivatives and primitives, providing constructive approximations for higher-dimensional composite functions—e.g., $f(g(x)h(y))$, $f(g''(x) \int h(y))$, etc.

The performance of the proposed algorithm is tested on a collection of univariate and multivariate functions. In the univariate scenario, the method demonstrates a stable convergence that matches the theoretical convergence rates. At the same time, it exhibits an efficient performance, requiring polynomial resources and avoiding the curse of dimensionality. In particular, its runtime scales close to linearly with the approximation order and sub-linearly with the number of qubits, hence sub-logarithmically with the density of the discretization. Moreover, the method generalizes to the multivariate scenario maintaining its accurate convergence rates

and polynomial resource requirements.

Despite this, in the univariate scenario the algorithm generally does not outperform tensor cross-interpolation or multiscale interpolative constructions. This is particularly true when function evaluations are inexpensive or when the function is not highly-differentiable. However, it outperforms TCI in some multivariate scenarios, such as those that benefit from the interleaved qubit order. Moreover, the method generalizes for the composition of functions on generic MPS/QTT structures, a task where the remaining algorithms are less applicable. This capability is useful in scenarios such as non-linear problems [30] and many-body statistical physics [31]. In addition, the method can be applied in a straightforward manner to compose functions on generic matrix product operators (MPO).

This work is organized as follows: Section II presents the mapping between functions and MPS and the finite-precision non-linear algebra framework required to approximate the MPS operations. Section III introduces the Chebyshev approximation algorithm and its formulation in terms of MPS. Section IV benchmarks the Chebyshev expansion over a collection of univariate and multivariate functions, comparing the results with TCI and multiscale interpolative constructions. Finally, Section V discusses this work's results with a focus on applications and future extensions.

II. QUANTUM-INSPIRED NUMERICAL ANALYSIS

Low-dimensional, weakly entangled quantum states admit an efficient representation as matrix product states [32]. In this form, the exponentially large tensor of amplitudes of a quantum system with n components

$$|\psi\rangle = \sum_{s_1=1}^{d_1} \sum_{s_2=1}^{d_2} \cdots \sum_{s_n=1}^{d_n} \psi_{s_1 s_2 \dots s_n} |s_1, s_2, \dots, s_n\rangle \quad (1)$$

becomes a collection of mutually contracted tensors

$$\psi_{s_1 s_2 \dots s_n} = \sum_{\alpha_1=1}^{\chi_1} \sum_{\alpha_2=1}^{\chi_2} \cdots \sum_{\alpha_n=1}^{\chi_n} A_{\alpha_1}^{s_1} A_{\alpha_1 \alpha_2}^{s_2} \cdots A_{\alpha_n}^{s_n}, \quad (2)$$

where a product of matrices determines the individual amplitudes.

In Penrose's graphical notation [c.f. Figure 1], this decomposition is depicted as a one-dimensional train of boxes, where each box corresponds to a tensor, the lines that connect them represent contracted indices, α_i , and the free indices become freely standing "legs", s_i where $i = 1, \dots, n$.

By construction, the number of elements in a MPS grows polynomially with the number of components $\mathcal{O}(ns\chi_{\max}^2)$, where $\chi_{\max} = \max \chi_i$ is the largest "bond dimension". This bond dimension does not depend on

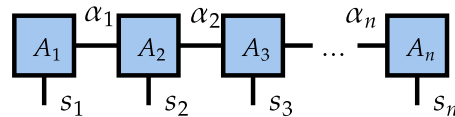


FIG. 1: Matrix product state composed of n mutually contracted rank-3 tensors A_i , with virtual indices α_i and physical indices s_i .

the system size for weakly entangled states. In those situations, the MPS representation is exponentially more efficient than the tensor representation $\psi_{s_1, s_2, \dots, s_n}$ of the quantum state. Let us now discuss how these improvements apply to the representation of functions.

A. MPS/QTT representation of functions

Besides aiding in the study of quantum many-body systems, MPS are useful for encoding multidimensional data. In the functional tensor train (FTT) formalism, a multivariate function is encoded as a tensor with one index per variable, and the result is decomposed into MPS form. This technique was independently discovered in quantum mechanics [33] and applied mathematics [34]. In the "quantized" or "quantics" tensor train (QTT) formalism, which is the focus of this work, each dimension uses multiple indices, enabling greater flexibility and efficiency. This technique has been rediscovered in multiple works from mathematics [8, 35] and quantum-inspired algorithms [9, 15, 30, 36].

The QTT transforms a discretized function into a tensor whose indices label the grid points. For a one-dimensional continuous variable x defined in an interval $[0, 1)$, a set of n digits (or indices) running over k values, $s_i \in \{0, 1, \dots, k-1\}$, can label up to k^n points. In particular, when the grid is uniform, a k -nary representation of the points is given by

$$x_{s_1 s_2 \dots s_n} = 0.s_1 s_2 \dots s_n = \sum_{i=1}^n s_i k^{-i}. \quad (3)$$

These k^n values may be regarded as a tensor with n indices, s_1 to s_n , each addressing progressively smaller length scales. The tensor encoding of the x coordinate generalizes to arbitrary univariate functions

$$f_{s_1 s_2 \dots s_n} := f(x_{s_1 s_2 \dots s_n}), \quad (4)$$

as well as extend to multidimensional functions, with the caveat that we now have multiple choices for the ordering of indices [9]. In this work we use either a sequential or serial order

$$g_{s_1^1 s_1^2 \dots s_1^n \dots s_2^1 s_2^2 \dots s_2^n \dots s_n^1 s_n^2 \dots s_n^n} = g(x_{s_1^1 s_1^2 \dots s_1^n}, \dots, x_{s_n^1 s_n^2 \dots s_n^n}), \quad (5)$$

and an interleaved order

$$g_{s_1^1 \dots s_1^d s_2^1 \dots s_2^d \dots s_n^1 \dots s_n^d} = g(x_{s_1^1 s_1^2 \dots s_1^d}, \dots, x_{s_n^1 s_n^2 \dots s_n^d}). \quad (6)$$

All these tensors are amenable to an MPS/QTT decomposition (2) with an efficiency that is determined by their bond dimension structure. Often, their “compressibility” depends on factors such as the algebraic structure, smoothness, or displacement structure of the function [37]. Moreover, the bond dimensions also depend on the value of k , which in this work is taken to be $k = 2$, operating with two-dimensional “quantum” components or “qubits”.

Sufficiently smooth univariate functions are known to be highly compressible, as they yield a MPS/QTT with bounded entanglement entropy [9, 38]. In particular, polynomials of finite degree d admit an exact representation with $\chi_{\max} \leq d + 1$ [25] which can be constructed analytically as proven in Appendix A—unfortunately, this construction is ill-conditioned for constructing Chebyshev interpolants. Interestingly, Chebyshev polynomials discretized over the Chebyshev-Gauss nodes require a constant bond dimension $\chi_{\max} = 2$ [8]. Other canonical examples include the exponential function ($\chi_{\max} = 1$), the sine and cosine functions ($\chi_{\max} = 2$) and periodic vectors of period ℓ , which require $\chi_{\max} = \ell$.

In general, loading a function $f(x)$ in an MPS requires a specialized algorithm. A naïve approach discretizes the function on a tensor $f_{s_1 s_2 \dots s_n}$ and applies a sequence of singular value decompositions (SVD). This creates an MPS with an optimal error in Frobenius norm [23] using a time and memory that scale with the volume of the tensor. Fortunately, other algorithms exist with a logarithmic cost relative to the size of the discretization. As mentioned in the introduction, these methods are divided into those that require some randomized or induced sampling—e.g., tensor cross-interpolation methods (TCI) [23, 39–41] for both tensor-trains and for QTT [40, 42], and sketching methods [24]—and those that are based on some algebraic structure—such as rank-revealing interpolative constructions [25] and arithmetic circuit tensor networks [19].

This work proposes a different approximation technique that combines the benefits of interpolative formulas [25] with the algebraic structures of arithmetic circuit tensor networks [19]. It is based on a finite-precision non-linear algebra supporting function multiplication and addition in the MPS formalism, using it to implement a Chebyshev approximation scheme. The resulting algorithm creates algebraic structures for individual functions of one $f(x)$ or more variables $f(x, y, z)$, which can be composed in arbitrary ways, such as $f(g(x))$ or $f(g(x) + h(y))$, etc. This approach has the benefit of generalizing to multiple dimensions, going beyond examples that result from tensorization of univariate functions [37, 43].

B. Finite-precision non-linear algebra

Let us endow the space of matrix product states with three non-linear operations. The fundamental one is the

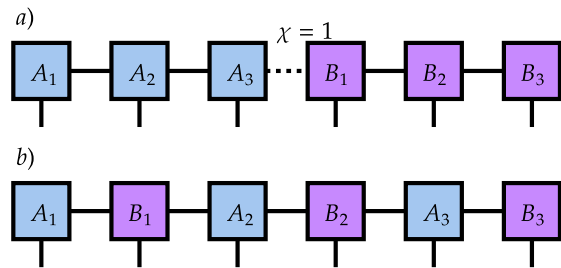


FIG. 2: Illustration of the tensor product of two MPS $|A\rangle$ and $|B\rangle$ in serial (a) and interleaved (b) orders.

approximation of a linear combination of MPS by another with potential limits on the size and complexity of its tensors. Formally, a state

$$|\phi\rangle = \operatorname{argmin}_{\phi \in \text{MPS}} \left\| |\phi\rangle - \sum_{i=1}^L \alpha_i |\psi_i\rangle \right\|_2^2, \quad (7)$$

is searched over the set MPS of matrix product states with maximum bond dimension χ . This work uses a two-site variational truncation scheme parameterized by a tolerance ϵ that controls the maximum error, as detailed in Refs. [9, 16]. The second operation is the element-wise product of MPS, resulting from the the non-linear multiplication of the vector elements

$$|u\rangle \cdot |v\rangle := \sum_{s_1, s_2, \dots, s_n} u_{s_1 s_2 \dots s_n} v_{s_1 s_2 \dots s_n} |s_1, s_2, \dots, s_n\rangle. \quad (8)$$

The third operation is the tensor product of two MPS. This is a straightforward operation based on tensor concatenation that combines the two Hilbert spaces. These tensors can be concatenated following a serial or interleaved order [c.f. Figure 2].

$$|x\rangle \otimes |y\rangle := \sum_{\vec{s}, \vec{r}} x_{s_1 \dots s_n} y_{r_1 \dots r_n} |s_1, \dots, s_n, r_1, \dots, r_n\rangle, \\ |x\rangle \otimes |y\rangle := \sum_{\vec{r}, \vec{s}} x_{s_1 \dots s_n} y_{r_1 \dots r_n} |s_1, r_1, \dots, s_n, r_n\rangle. \quad (9)$$

The complexity of the resulting state depends on the structure of its correlations [9].

III. CHEBYSHEV APPROXIMATION

Any continuous univariate function can be approximated by a polynomial up to a given order. The Chebyshev polynomials form a convenient basis [27, 28] that results in a close to optimal approximation—the minimax polynomial—hence providing excellent convergence guarantees, i.e., exponential and algebraic decay of errors for analytical and differentiable functions. This technique is commonly used within pseudospectral methods for the

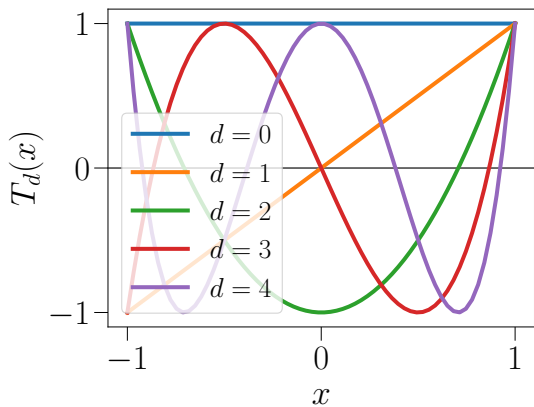


FIG. 3: Representation of the first five Chebyshev polynomials.

numerical solution of partial differential equations [44]. In this section, this method is adapted to approximate MPS/QTT representations of functions using the finite-precision non-linear algebra framework from Section IIa. This adaptation involves understanding the convergence guarantees, MPS complexity estimates, and optimal evaluation orders.

A. Expansion on the Chebyshev basis

The Chebyshev polynomials of the first kind [c.f. Fig. 3] are monic polynomials $T_k(x) : [-1, 1] \rightarrow [-1, 1]$ defined by the trigonometric relation $T_k(\cos \theta) = \cos(k\theta)$, $k \in \mathbb{N}$. They are orthogonal with respect to the weight function $\omega(x) = 1/\sqrt{1-x^2}$

$$\int_{-1}^1 T_k(x)T_l(x)\omega(x)dx = \frac{\pi}{2}(1 + \delta_{k0})\delta_{kl} \quad (10)$$

and they satisfy a three-term recurrence relation

$$T_{k+1}(x) = 2xT_k(x) - T_{k-1}(x), \quad k \geq 1 \quad (11)$$

with $T_0(x) = 1$, $T_1(x) = x$.

Any continuous function $f(x)$ defined in $[-1, 1]$ shows a convergent series in the Chebyshev basis, as

$$f(x) = \sum_{k=0}^{\infty} a_k T_k(x), \quad \text{with} \quad (12)$$

$$a_k = \frac{2 - \delta_{k0}}{\pi} \int_{-1}^1 f(x)T_k(x)\omega(x)dx. \quad (13)$$

The Chebyshev projection of order d is the d -th order polynomial that results from truncating (12) up to the first $d+1$ terms $f_d(x) = \sum_{k=0}^d a_k T_k(x)$. These expansions can be trivially generalized to functions in other intervals $g(u) : [a, b] \rightarrow \mathbb{C}$, via the affine transformation

$$u = \alpha x + \beta, \quad (14)$$

with $\alpha = (a - b)/2$, and $\beta = (a + b)/2$.

Alternatively, a function can be approximated by the interpolation on either the Chebyshev-Gauss nodes, given by the d zeros of the d -th order Chebyshev polynomials $r_k \in (-1, 1)$,

$$r_k = \cos\left(\frac{\pi(2k-1)}{2d}\right), \quad k = 1, 2, 3, \dots, d, \quad (15)$$

or the Chebyshev-Lobatto nodes, given by the $d+1$ extrema of $T_d(x)$ in the closed set $[-1, 1]$

$$\ell_k = \cos\left(\frac{k\pi}{d}\right), \quad k = 0, 1, 2, \dots, d. \quad (16)$$

The new interpolant is the polynomial series that results from evaluating the interpolated function on the chosen set of nodes [28]. For the case of Chebyshev-Gauss nodes,

$$p_d(x) = \sum_{k=0}^d c_k T_k(x), \quad \text{with } c_k = \frac{2}{d} \sum_{i=1}^d {}'f(r_i)T_k(r_i), \quad (17)$$

where the primed sum involves halving the term $i = 1$.

The coefficients c_k can be computed from a discrete cosine transform (DCT)

$$c_k = \text{DCT}\{f(r_k)\}, \quad (18)$$

which may be implemented with $\mathcal{O}(d \log d)$ cost using the fast Fourier transform.

These expansions may be generalized to the multidimensional scenario. However, in such case the coefficients become a tensor $c_{k_1 \dots k_m}$ that scales exponentially with the dimension and the contraction

$$f(x_1, \dots, x_m) = c_{k_1 \dots k_m} T_{k_1}(x_1) \dots T_{k_m}(x_m), \quad (19)$$

becomes computationally intractable. This complexity may be avoided for functions that result from the composition of other functions, such as $f(g(x)h(y))$. Also, the derivatives or primitives of a Chebyshev approximation follow from simple recurrence relations of its coefficients [27]. This enables the approximation of functions involving primitives or derivatives, such as $f(g''(x) \int h(y))$, that need not have a closed analytical form.

B. Convergence properties

The rate of convergence of polynomial approximations is usually measured in terms of the distance in L^∞ norm, also known as the Chebyshev norm, between the function and its approximant. This distance is defined as the limit of

$$\|f(x) - g(x)\|_p = \left(\int_{-\infty}^{\infty} |f(x) - g(x)|^p dx \right)^{1/p} \quad (20)$$

when $p \rightarrow \infty$, and corresponds to the maximum point-wise error

$$\|f(x) - g(x)\|_\infty = \max_x |f(x) - g(x)|. \quad (21)$$

In practice, the functions are discretized on a grid with N points, resulting in the estimation

$$\|f(x) - g(x)\|_p^{(N)} = \left(\frac{1}{N} \sum_{i=1}^N |f(x_i) - g(x_i)|^p \right)^{1/p}. \quad (22)$$

The convergence of a Chebyshev interpolant (17) is determined by the decay rate of its Gibbs oscillations in between the interpolated nodes. These depend on the smoothness properties of the approximated function. Models with a finite number of derivatives and analytical functions converge algebraically and exponentially fast with the expansion order, respectively [28].

Theorem 1 *For an integer $\nu \geq 0$, let f and its derivatives through $f^{(\nu-1)}$ be absolutely continuous on $[-1, 1]$ and suppose the ν -th derivative $f^{(\nu)}$ is of bounded variation V . Then for any interpolation order $d > \nu$, its Chebyshev interpolants p_d satisfy*

$$\|f - p_d\|_\infty \leq \frac{4V}{\pi\nu(d-\nu)^\nu}.$$

Theorem 2 *Let a function f analytic in $[-1, 1]$ be analytically continuable to the open Bernstein ellipse E_ρ , where it satisfies $|f(x)| \leq M$ for some M . Then for each interpolation order $d \geq 0$ its Chebyshev interpolants p_d satisfy*

$$\|f - p_d\|_\infty \leq \frac{4M\rho^{-d}}{\rho - 1}.$$

C. Clenshaw's evaluation method

The evaluation of the partial sum (17) can pose numerical instabilities [27, 45, 46] and requires the additional computation of d Chebyshev polynomials. Both issues are simultaneously addressed by Clenshaw's evaluation method [45]. This method allows for the efficient evaluation of partial sums of orthogonal polynomials by expanding their three-term recurrence relation and keeping only the non-vanishing terms. For Chebyshev polynomials, it reduces the evaluation of the partial sum (17) to a linear combination $f(x) = y_0 - xy_1$, where the quantities y_j are defined according to the following inverse recurrence relation

$$\begin{aligned} y_{d+1} &= y_d = 0, \\ y_{n-1} &= c_{n-1} - y_{n+1} + 2xy_n, \text{ for } 2 < n \leq d \\ y_1 &= c_1 - y_3 + 2xy_2, \text{ and} \\ y_0 &= c_0 - y_2 + 2xy_1. \end{aligned} \quad (23)$$

Algorithm 1 MPS/QTT Chebyshev interpolation of $f(g(x))$ in the Chebyshev-Gauss nodes

Require: Univariate scalar function f , MPS initial condition $|g\rangle$ with support in $[a, b]$, interpolation order d , tolerance ϵ .

Compute the Chebyshev coefficients for f

$$\begin{aligned} \tilde{r}_k &\leftarrow \cos\left(\frac{\pi(2k-1)}{2d}\right), \quad k = 1, \dots, d \\ r_k &\leftarrow \text{AFFINE}(\tilde{r}_k, [-1, 1] \rightarrow [a, b]) \\ c_k &\leftarrow \text{DCT}(f(r_k)) \end{aligned}$$

Rescale the MPS argument

$$|\tilde{g}\rangle \leftarrow \text{AFFINE}(|g\rangle, [a, b] \rightarrow [-1, 1])$$

Perform the Clenshaw evaluation

$$\begin{aligned} n &\leftarrow \text{number of qubits in } |g\rangle \\ |\mathbf{I}\rangle &\leftarrow \text{Identity MPS with } n \text{ qubits} \\ |y_{d+1}\rangle, |y_d\rangle &\leftarrow \text{Zero MPS with } n \text{ qubits} \end{aligned}$$

for $k = d$ **to** 0 **do**

$$|y_k\rangle \leftarrow \text{SIMP}(c_k |\mathbf{I}\rangle - |y_{k+1}\rangle + 2|\tilde{g}\rangle \cdot |y_{k+1}\rangle; \epsilon)$$

end for

$$\text{return } \text{SIMP}(|y_0\rangle - |\tilde{g}\rangle \cdot |y_1\rangle; \epsilon)$$

D. Chebyshev approximation with MPS/QTT

The partial sum (17) and its equivalent formulation using Clenshaw's method (23) require the identity and an initial condition x . These primitives can be efficiently loaded in MPS using the recipe shown in Appendix A. Therefore, the partial sum can be reformulated as

$$|p_d(x)\rangle = \sum_{k=0}^d c_k |T_k(x)\rangle, \quad (24)$$

where the MPS Chebyshev polynomials are computed following their recurrence relation

$$|T_{k+1}(x)\rangle = 2|x\rangle \cdot |T_k(x)\rangle - |T_{k-1}(x)\rangle. \quad (25)$$

These expressions depend only on the identity state $|\mathbf{1}\rangle$ and the initial condition $|x\rangle$, as well as on linear combinations and product operations. To avoid an unbounded growth of the bond dimension, the intermediate states of the approximation shall be periodically simplified. Equivalently, the Clenshaw evaluation (23) can be reformulated in terms of a sequence of MPS $|y_n\rangle$ and a linear combination $|f\rangle = |y_0\rangle - |x\rangle \cdot |y_1\rangle$. As shown in Appendix B, this approach proves to be more efficient and robust than the standard evaluation.

The steps required to compute the MPS Chebyshev approximation of a function composition $f(g(x))$ on the Chebyshev-Gauss nodes (15) are summarized in Algorithm 1. There, $g(x)$ is given as a prior MPS representation $|g\rangle$. This algorithm specializes in loading functions $f(x)$ by making $g(x) = x$, and generalizes as a method for function composition, extending earlier MPS algebraic

frameworks[19]. This approach has the caveat of needing to know the support of $g(x)$ in order to rescale it to fit in the domain of the Chebyshev expansion $[-1, 1]$ using an efficient affine transformation. The algorithm relies on the simplification routine, referred as SIMP and parametrized by a tolerance ϵ , to perform the linear combinations of MPS and their subsequent simplification. Note that this approach may encounter numerical instabilities for large MPS.

The cost of Chebyshev expansions and function composition is dominated by the variational simplification routine, which scales as $\mathcal{O}(\chi^3)$ for every tensor of the simplified state. Since the intermediate states are polynomials of degree $k \leq d$, this sets a complexity upper bound of $\mathcal{O}(\sum_{k=0}^d (k+1)^3) = \mathcal{O}(d^4)$. However, in practice the bond dimension structure of the intermediate states allows for a much better performance.

IV. NUMERICAL BENCHMARKS

This section evaluates the performance of the MPS/QTTChebyshev approximation for loading collection of univariate and multivariate functions. The figures of merit are the error in discretized L^∞ norm (22), the maximum bond dimension χ_{\max} of the representation—a proxy for the memory requirements given by the $\mathcal{O}(2\chi_{\max}^2)$ scaling—and the runtime of the algorithm. These metrics are computed for different parameter sets, defined by the number n of qubits of the representation, the polynomial order d and the tolerance ϵ that parametrizes the intermediate simplification steps. A comprehensive study requires nine independent experiments. These are organized in three columns of mutually shared axes.

The performance of MPS Chebyshev expansions will be compared with two state-of-the-art techniques: multiscale interpolative constructions, as devised by Lindsey [25], and tensor cross-interpolation (TCI) [23]. The description of the TCI algorithm employed in this work, as well as the implementation details, are presented in Appendix C.

A. Univariate functions

All algorithms are tested on a set of qualitatively different one-dimensional functions, shown in Figure 4. The first two are the Gaussian distribution

$$f_G(x; \sigma) = \frac{1}{\sigma\sqrt{2\pi}} e^{-\left(\frac{x}{2\sigma}\right)^2} \quad (26)$$

with $\sigma = 1/3$, and a highly-oscillatory function

$$f_O(x; \varepsilon) = \cos\left(\frac{1}{x^2 + \varepsilon}\right) \quad (27)$$

with $\varepsilon = 10^{-2}$. Both are analytical functions and are expected to exhibit an exponential convergence rate with

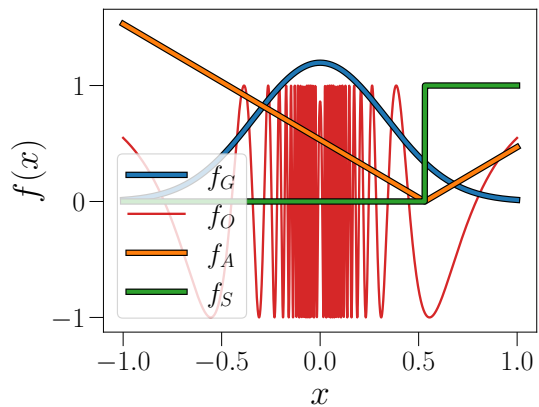


FIG. 4: Four qualitatively different functions proposed for the univariate performance evaluation of the different methods. The color code labeling each function is preserved along the subsequent studies. In blue, a Gaussian probability distribution f_G (26). In red, an oscillating function f_O (27). In orange, the absolute value function f_A (28). Lastly, in green, the Heaviside step function f_S (29).

the interpolation order d after a sufficiently large plateau of errors. The other two functions are non-smooth, allowing to explore the limitations of polynomial approximations compared to TCI. These include the absolute value function

$$f_A(x; x_c) = |x - x_c|, \quad (28)$$

and the Heaviside step function

$$f_S(x; x_c) = \Theta(x - x_c). \quad (29)$$

These functions are centered on an offset grid point $x_c = \frac{1}{2} + \frac{1}{25}$ to avoid considering some artificially simple representations. The Heaviside step function is discontinuous, so its Chebyshev expansion exhibits constant Gibbs oscillations that lead to a finite error. The absolute value function has only first-order derivatives of bounded variation, leading to an inefficient algebraic attenuation of its Gibbs oscillations.

1. MPS/QTTChebyshev approximation

The study explores grids with up to 2^{25} points—i.e., $n = 25$ qubits—and a numerical tolerance of up to $\epsilon = 10^{-14}$, leading to a truncation error close to machine precision. The interpolation order d runs up to 1300 for all functions, except for the Gaussian function, which requires a maximum of $d = 50$ in order to prevent a degradation of the accuracy of the Clenshaw method, as detailed in Appendix B. The results are grouped in Figure 5, where they are addressed and interpreted column-wise.

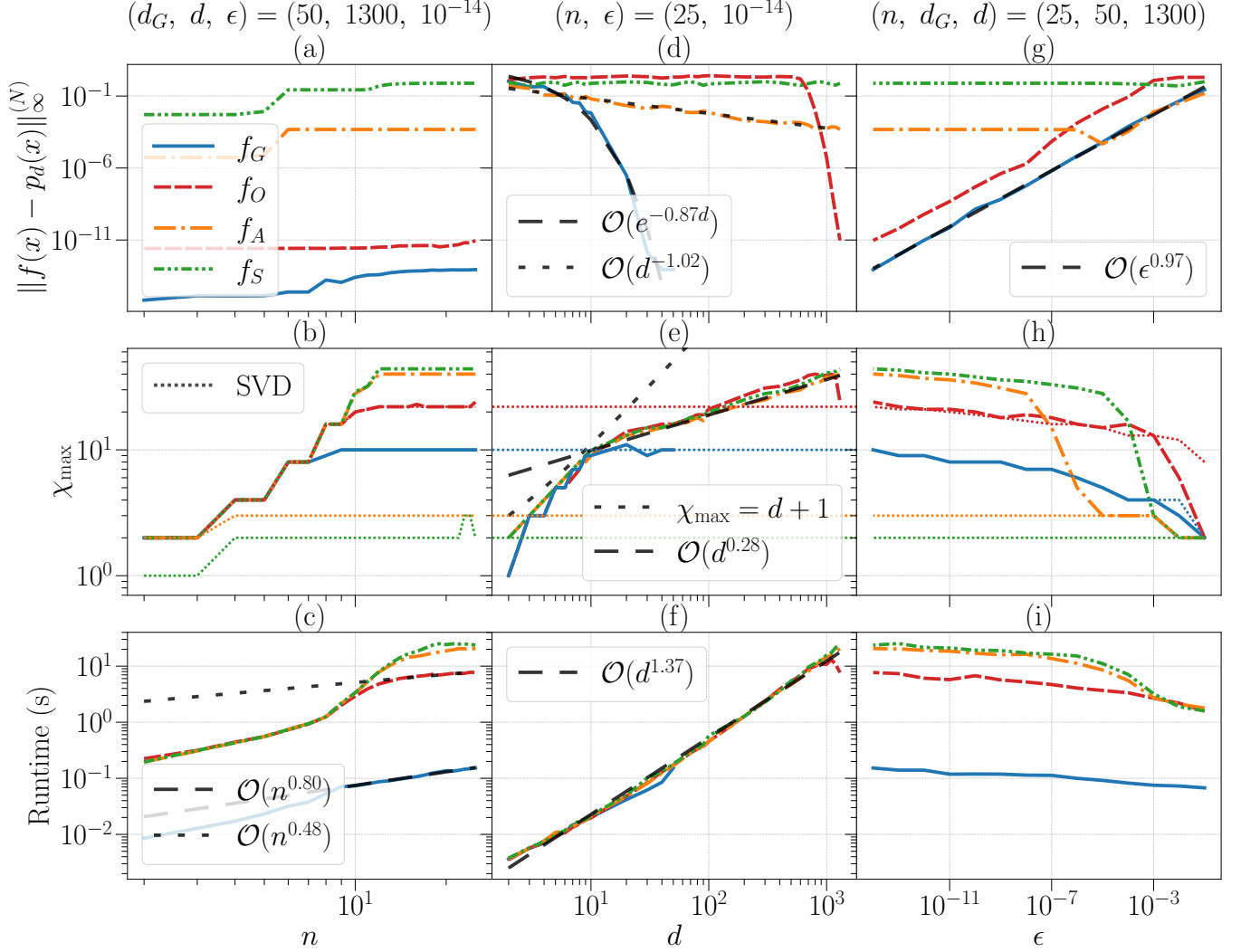


FIG. 5: Results for the MPS/QTT Chebyshev approximation of the four univariate functions f_G (26), f_O (27), f_A (28) and f_S (29). This study considers nine independent experiments given by the combination of the three parameter settings with the three figures of merit. All axes are mutually shared and shown in logarithmic scale. The second row contains a thin dotted curve representing the maximum bond dimension of a SVD decomposition. The results are asymptotically fitted with thick dashed curves and the scalings are shown in the legend. The main messages of the results can be understood by columns. The first column suggests that MPS polynomial approximations are of low entanglement, as their bond dimensions saturate to a value that is independent of the grid and only function-dependent. The second column illustrates that the method converges according to the theoretical rates for Chebyshev expansions, but with a complexity that scales algebraically below the bound for MPS polynomials. The third column demonstrates that the local truncation error of the MPS, given by the tolerance ϵ , provides a good proxy for the error and complexity entailed in the approximations.

The first column addresses the representability of the functions as MPS by setting the order of the expansion and tolerance ϵ to the most precise values, and evaluating the effects of the grid size on the L^∞ norm, maximal bond dimension and CPU time, as respectively shown in Figures 5(a), 5(b) and 5(c). The results depict that the L^∞ norm is a smooth function of the grid spacing and converges for grids involving a few thousand points, for which the maximal bond dimension saturates

to a value that only depends on the specific function— a manifestation of the bounded entanglement content of polynomials—. Also, it matches those of the optimal decomposition of the tensor $f_{s_1 s_2 \dots s_n}$ using the iterative SVD for the two analytical functions. The computational cost scales sublinearly, with an averaged rate of $\mathcal{O}(n^{0.64 \pm 0.16})$, as the tensors corresponding to the less significant bits asymptotically converge to a reduced bond dimension [25]. This decay can be interpreted to mean

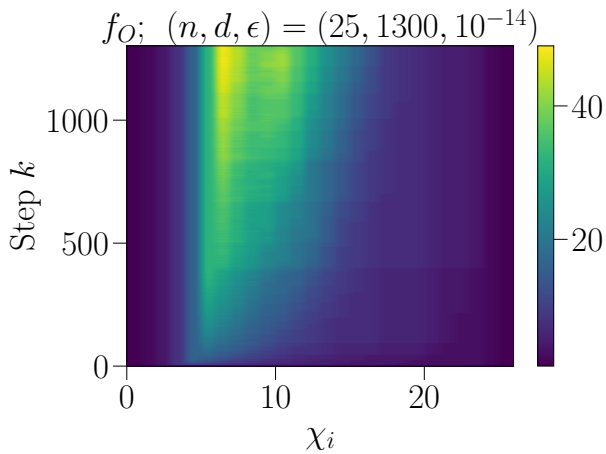


FIG. 6: Bond dimension structure of the MPS corresponding to the oscillating function f_O (27) for each of the 1300 intermediate Clenshaw evaluation steps. A similar behavior is noted and omitted for the remaining test functions. The bond dimension varies noticeable with the position in the chain, meaning that we never have to deal with a square MPS tensor, and as a result the computational cost of the full algorithm is much lower than the expected χ_{\max}^3 required to perform an SVD decomposition of a $\chi_{\max} \times \chi_{\max}$ matrix.

that, at those scales, the polynomial approximations of sufficiently well-behaved functions can be interpolated almost linearly, even if we are approximating non-smooth functions. This decay is demonstrated for every intermediate step in Figure 6.

The second column in Figure 5 evaluates the effects of the interpolation order for the finest grid with 2^{25} nodes. Figure 5(d) demonstrates that the approximations converge according to the theoretical expectations of Theorems 1 and 2. Moreover, Figure 5(e) shows that the maximum bond dimension scales sub-linearly with the interpolation order as $\mathcal{O}(d^{0.28})$ for all test functions. This curve lays systematically below the polynomial upper bound of $\chi_{\max} = d+1$ known for d -th order polynomials [c.f. Appendix A]. At convergence, this bond dimension is consistent with the optimal SVD value, as shown for the Gaussian and oscillatory functions for $d_G = 50$ and $d = 1300$, respectively. Finally, Figure 5(h) shows how the computational cost scales at a close-to-linear rate of $\mathcal{O}(d^{1.37})$ with the interpolation order, well below the expected worst case scenario of $\mathcal{O}(d^4)$. Again, this is attributed to the intermediate bond dimension structure of the MPS approximations shown in Figure 6. As the MPS tensors are highly rectangular, the expected $\mathcal{O}(d^3)$ cost for SVD is subleading.

Finally, the third column analyzes whether the truncation error at each step acts as an indicator of the global approximation error. Figures 5(g), 5(h) and 5(i) illustrate that the global approximation error, maximal bond dimension and CPU time are parameterized by

the tolerance parameter ϵ . In particular, the global error is a monotonically decreasing function of ϵ until it is dominated by the error of the expansion. Furthermore, the maximal bond dimension increases mildly—logarithmically—with the tolerance parameter for all functions. This parametrization allows exploring the tradeoffs between accuracy and computational cost when a good Chebyshev expansion is warranted.

Based on these results, the MPS/QTTChebyshev approximation proves to be an efficient method for loading highly-differentiable univariate functions. It offers a reliable performance for a large numbers of qubits, attributed to the advantageous bond dimension structure of the intermediate steps and demonstrated by its sub-logarithmic scaling with discretization size. Moreover, it exhibits excellent error guarantees for smooth and highly-differentiable functions that align with the theoretical bounds. This motivates its generalization to multivariate problems. However, before addressing this scenario, it is of interest to compare it against other state-of-the-art methods for loading functions, such as multiscale interpolative constructions [25] and TCI.

2. Multiscale interpolative constructions

In the one dimensional case there exist alternative methods to construct the MPS representation of a Chebyshev interpolant. Notably, M. Lindsey has developed several variants of a multiscale interpolative construct based on Lagrange interpolation [25], which shall be compared with the previous iterative algorithm.

In the following, we briefly summarize the spirit of this technique, and refer the interested reader to the original paper. Essentially, the basic construct builds an MPS interpolant in a single pass. It begins by assembling a left-most tensor core that captures the information of the values of a function $f(x)$ on two Chebyshev-Lobatto grids (16), each with $d+1$ points and sharing the intersection. This procedure constructs an effective interpolant by joining two interpolants of order $d+1$ and using $2d+1$ function values. Then, two additional tensor cores are assembled belonging to the bulk and right-most edges of the MPS. These cores propagate the function information and implement the Lagrange interpolating polynomial. Once they are assembled, these cores can be reused for subsequent interpolations. Hence, this interpolation procedure is universal, given that different functions only differ in the first tensor while all the subsequent ones are the same. The resulting state has all bond dimensions set to $\chi = d+1$ at maximum, which is a large overestimation and benefits from a simplification at the end of the algorithm. However, the same fundamental algorithm may be implemented in a rank-revealing form, where the tensor cores from the basic construct are simplified along the way using the SVD with a given tolerance ϵ , avoiding the need for a large-scale final simplification. Additionally, this algorithm can be reformulated using local Lagrange

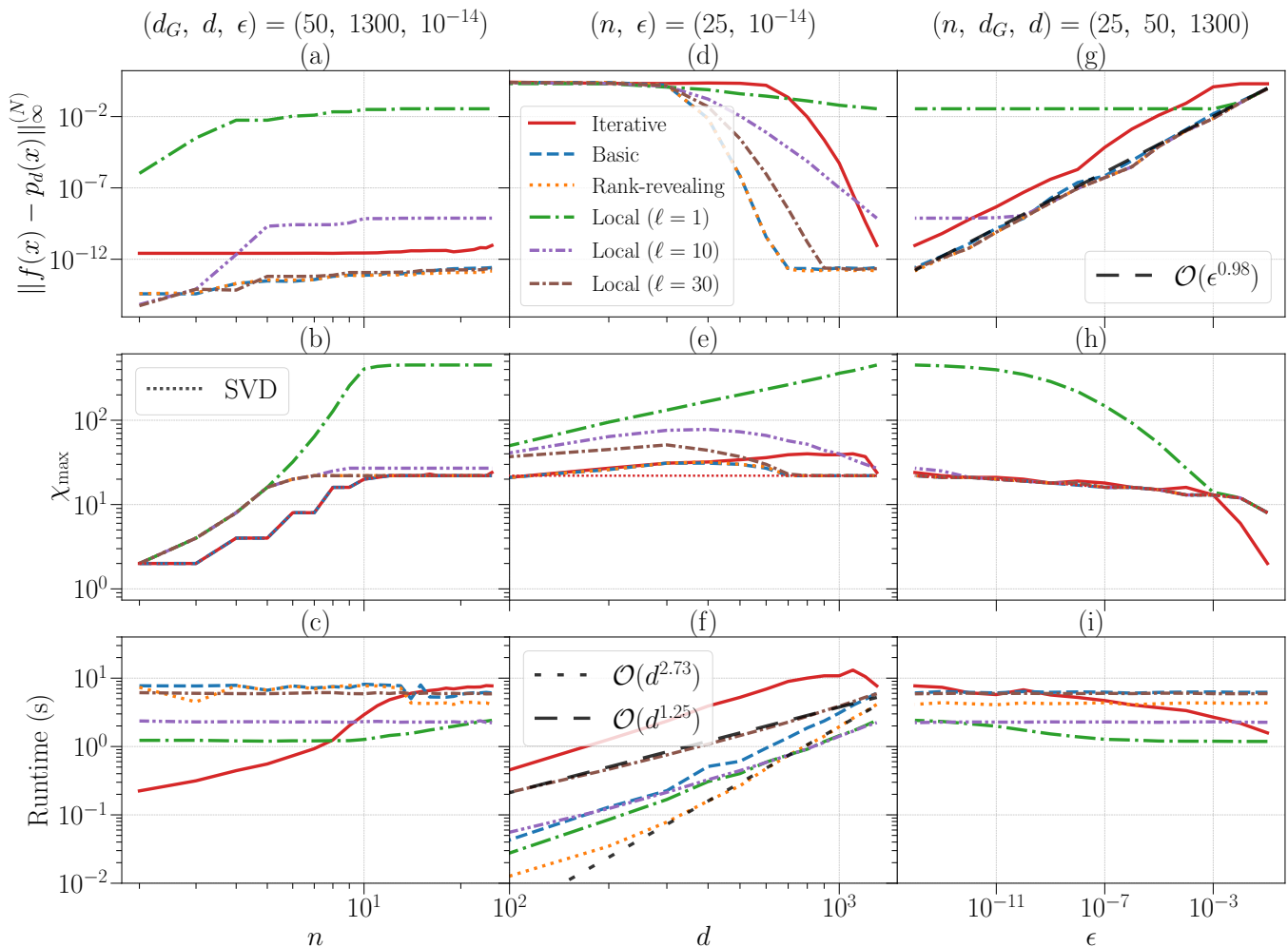


FIG. 7: Results for the three variants of multiscale interpolative constructions for the oscillating function (27). The results of MPS/QTT Chebyshev approximation are incorporated as a red solid baseline. The variation based on local interpolation is repeated for local orders $\ell = 1, 10, 30$. The results follow a similar structure than the previous study for the MPS/QTT Chebyshev approximation algorithm, shown in Figure 5.

interpolation with a specified local order ℓ . Then, the tensor cores become sparse improving the efficiency of tensor decompositions and contractions.

The parameters of all these variants are similar to those of the previous iterative algorithm, which enables a similar study. However, for simplicity and in order to analyze all algorithmic variants, the study focuses only on the oscillatory function (27), which is the most complex example given for the MPS Chebyshev expansion. The results are presented in Figure 7, where the outcome of the previous study is incorporated as a reference line in red color with the label “Iterative”.

As shown in Figure 7(a), global interpolative constructions converge accurately and stably with the number of qubits. However, local constructions require a large enough local order of approximately above $\ell = 10$ to do so, given that small enough local orders lead to a large deterioration of the convergence and maximum bond di-

mension as shown in Figures 7(a) and 7(b). Interestingly, Figures 7(d) and 7(e) demonstrate that these constructions converge with half the polynomial order than MPS Chebyshev expansions. This is due to the non-linear convergence rates of the two interpolants at each Chebyshev-Lobatto grid, spanning each half of the interval with $\lfloor \frac{d}{2} \rfloor - 1$ nodes.

The complexity of the interpolative construct is dominated by the assembly of the left-most, bulk and right-most cores. Hence, the algorithm’s performance almost does not scale with the system size, as shown in Figure 7(c). However, the resources required for the assembly scale with the interpolation order d with a rate that depends on the interpolation variant. As illustrated in Figure 7(f), the rate for the rank-revealing construction is close to cubic, as $\mathcal{O}(d^{2.73})$, while local constructions exhibit a slower rate, concretely of $\mathcal{O}(d^{1.25})$ for $\ell = 30$. The former rate surpasses the close-to-linear rate of $\mathcal{O}(d^{1.37})$

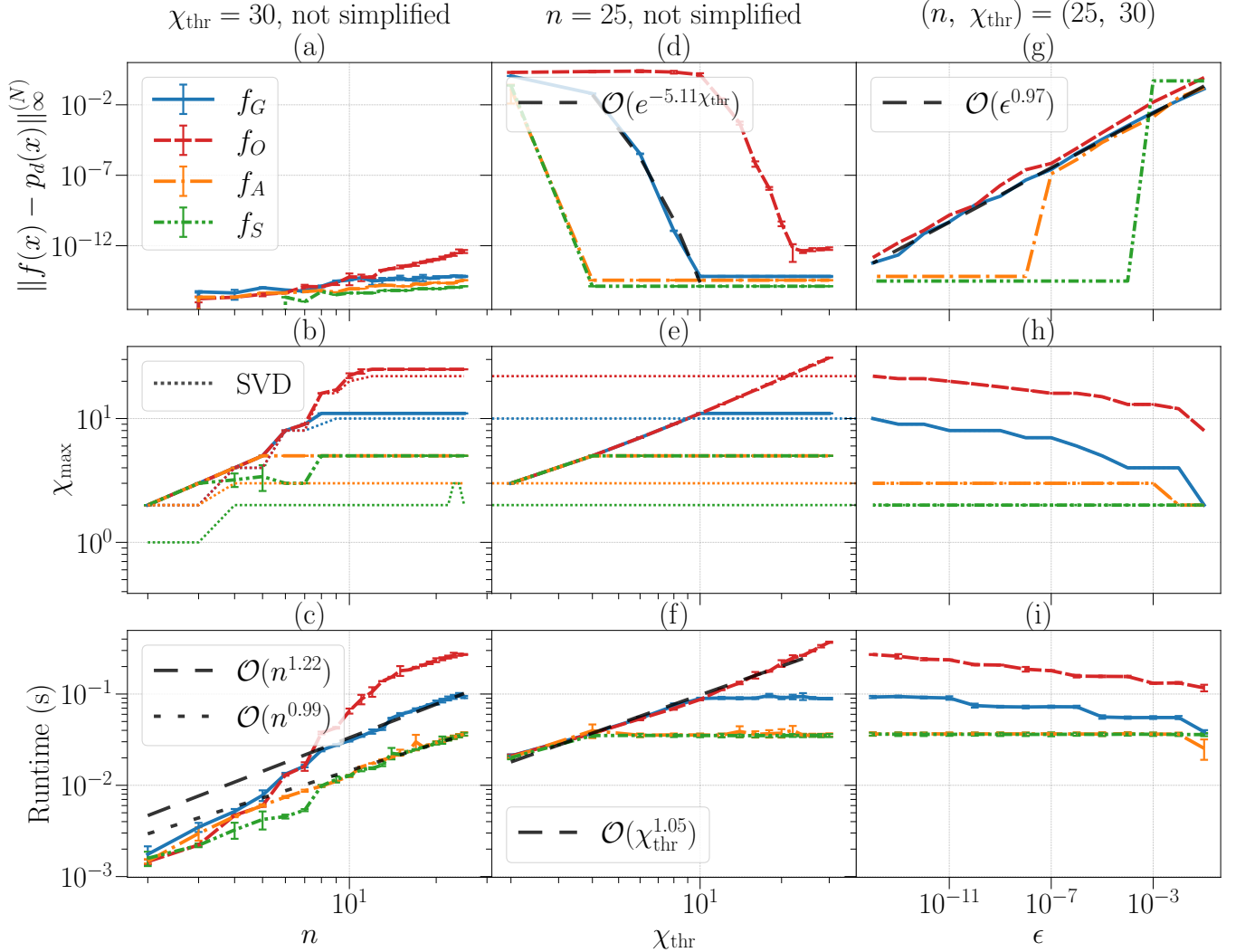


FIG. 8: Results for the tensor cross-interpolation of the four univariate functions f_G (26), f_O (27), f_A (28) and f_S (29). The results follow a similar structure than the previous studies for the MPS/QTTChebyshev approximation and multiscale interpolative constructions, shown respectively in Figure 5 and Figure 7.

of the previous algorithm shown in Figure 5(h). Nevertheless, we note that these rates may depend on specific implementation choices. In any case, Figures 7(c) and 7(i) suggest that the interpolative constructions outperform the iterative expansion for this function for $n \geq 10$, exhibiting lower CPU times within one order of magnitude. Finally, Figures 7(g), 7(h) and 7(i) illustrate how these algorithms can be similarly parameterized by the tolerance parameter of the simplification routine.

3. Tensor cross-interpolation (TCI)

Tensor cross-interpolation (TCI) is a state-of-the-art technique that constructs the tensor-train representation of a black-box function by sampling its elements. As opposed to the previous algorithms, TCI does not create a

polynomial or algebraic structure that can be reused, but rather samples the target function (or tensor) to get the smallest tensor cores that minimize a given cost function. The details of TCI as well as the particular implementation used in this work are detailed in Appendix C.

Essentially, TCI iteratively optimizes an initial MPS approximation of the function—which may start from a random guess. This optimization is done following “sweeps” that increase its bond dimension until convergence is achieved. In our suboptimal but performant implementation, the bond dimension grows with each sweep by 2, and is bounded by a predefined threshold value χ_{thr} . The relation between the order of polynomials and the maximum bond dimension [c.f. Appendix A] suggests that the threshold χ_{thr} may be considered analogous to the polynomial order d of the previous methods. Despite this upper limit, the algorithm is designed to halt when

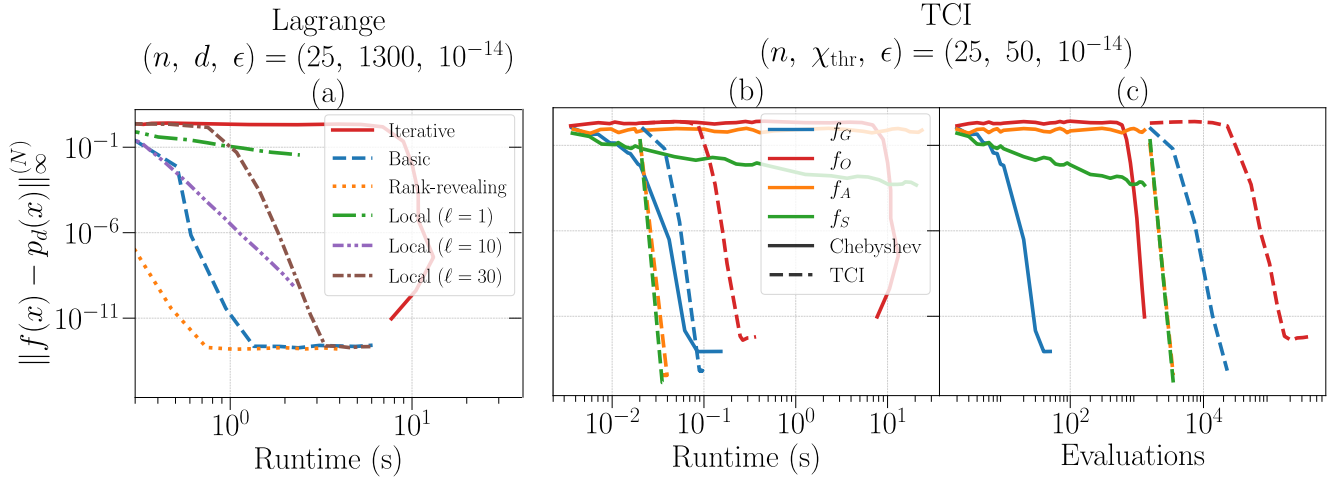


FIG. 9: Benchmark for univariate function loading using MPS Chebyshev approximations, multiscale interpolative constructions and TCI. The results compare the required runtime and number of function evaluations required to achieve a given approximation error. On the one hand, Figure (a) compares the performance of MPS Chebyshev approximation with the three variants of multiscale interpolative constructions for the oscillating function (27). On the other hand, Figures (b) and (c) compare the performance of MPS Chebyshev approximations (solid line) and TCI (dashed line) for the four univariate functions, with respect to both the required runtime and number of function evaluations.

the approximation error in L^∞ norm (21) falls below a predefined value. Interestingly, as TCI does not perform a polynomial approximation, it is not constrained by the smoothness of the target function and can in fact load non-differentiable targets efficiently.

This study replicates the analysis from Sect. IV A 1 up to a maximum bond dimension $\chi_{\text{thr}} = 30$ and a halting approximation error of ϵ . By default, the resulting MPS is not simplified with a tolerance ϵ . However, a final simplification with tolerance ϵ is considered in order to replicate the results shown in the third column of the previous studies. As the outcome now depend on a random initial condition, they are evaluated 10 times to extract the mean and standard deviation.

The results are presented in Figure 8. As shown in Figures 8(a) and 8(d), TCI achieves machine precision convergence for all test functions, even for non-differentiable targets, exhibiting an exponential convergence with greater rates than the previous algorithms. Figures 8(b) and 8(e) show how the complexities resemble those computed with SVD, while Figures 8(c) and 8(f) illustrate that asymptotic time scaling of TCI is close to linear with both the number of qubits and the threshold bond dimension. Hence, the required computational time shows an averaged scaling rate of $\mathcal{O}(n^{1.11 \pm 0.1})$ with the number of qubits, which is less favorable than the sublinear rate of the MPS/QTTChebyshev approximation and the constant rate of multiscale interpolative constructions.

4. Performance benchmark

The previous studies suggest that the three algorithms are capable of loading smooth univariate functions in MPS accurately and efficiently, avoiding the curse of dimensionality. However, TCI provides an exponential advantage in the representation of non-smooth functions. Moreover, the algorithms show different scaling rates. This section compares their performance explicitly.

The results are presented in Figure 9. Figure 9(a) compares the runtime required to achieve a given error between the iterative MPS/QTTChebyshev approximation and the multiscale interpolative constructions for the oscillating function (27) for different values of the order d . Similarly, Figures 9(b) and 9(c) benchmark MPS Chebyshev expansions and TCI for all test functions, also considering the number of required function evaluations.

As expected, all three methods converge exponentially for the analytical functions but differ in the prefactors of the overall scaling. Figure 9(a) illustrates how the constructive methods outperform the iterative Chebyshev approximation for the oscillating function within one order of magnitude. Similarly, Figure 9(b) shows that TCI outperforms the iterative method within more than one order of magnitude, due to its superior convergence rate. Also, it shows an exponentially better performance for the non-smooth functions. However, it underperforms for the Gaussian function, which requires a much lower interpolation order to converge. The performance gaps can be qualitatively attributed to the total information brought into the sampling. As shown in Figure 9(c), TCI uses approximately two orders of magnitude more evalu-

ations than the iterative expansion.

Despite these performance gaps, all three approximation techniques load smooth univariate functions with comparable accuracy. In this context, the function composition capabilities of the iterative Chebyshev algorithm enable tasks beyond function loading. These capabilities have no straightforward analogue using interpolative constructions, and require expensive state samples involving costly tensor contractions for the case of TCI. In contrast, the iterative Chebyshev approximation requires fewer inexpensive function evaluations.

B. Multivariate functions

The performance of the MPS/QTT Chebyshev approximation for loading univariate functions motivates its generalization to the multivariate scenario. In general, this requires creating an m -dimensional tensor of coefficients with an exponential cost (19). However, this can be avoided if the functions have a simple algebraic structure that can be derived from the composition of univariate functions. The goal of this study is to confirm the applicability of the MPS function algebra from Sect. II and the Chebyshev expansion to achieve a complete algebraic framework for function loading [19] that generalizes to more complex arbitrary functions and MPS/QTT encodings, while at the same time comparing the performance with the state-of-the-art.

This hypothesis is explored using two target functions: an ordinary Gaussian

$$f_{\text{product}}(\mathbf{x}) = \exp\left(\sum_{i=1}^m x_i^2\right), \quad (30)$$

and a *squeezed Gaussian*

$$f_{\text{squeezed}}(\mathbf{x}) = \exp\left(\left[\sum_{i=1}^m x_i\right]^2\right). \quad (31)$$

Both functions can be respectively understood as the composition of the exponential $h(x) = \exp(-x)$ with two polynomials, which are $\sum_i x_i^2$ and $(\sum_i x_i)^2$. Hence, both can be obtained by evaluating the MPS/QTT Chebyshev expansion of $h(x)$ on either of these polynomials—which have an efficient MPS representation combining the recipe of Appendix A with tensor products.

The study explores the performance of this composition strategy on problems with growing dimensionality, following a similar structure to previous studies with univariate functions. The dimension of the function, m , ranges between 1 and 10, and the tolerance of the intermediate simplifications is varied between 10^{-1} and 10^{-14} . The results are compared against TCI for the same multivariate functions. However, since TCI enables loading non-smooth functions accurately, we also benchmark this

method against the multivariate generalization of f_A (28) and f_S (29),

$$f_{A,m}(\mathbf{x}; x_c) = \left| \sum_{i=1}^m x_i - x_c \right|, \quad \text{and} \quad (32)$$

$$f_{S,m}(\mathbf{x}; x_c) = \Theta\left(\sum_{i=1}^m x_i - x_c\right). \quad (33)$$

Note that, as explained in Sect. II, there are many different orderings of qubits in a multidimensional tensorized encoding. The study analyzes sequential and interleaved orders from Fig. 2.

The largest problem involves 10 variables with 20 qubits each, resulting in a Hilbert space with $\sim 10^{60}$ elements. This makes the computation of the error in discretized L^∞ norm intractable. Hence, this error is estimated using standard Monte Carlo sampling techniques. This estimation is assessed to converge to the full-tensor error for a moderate amount of function samples in Appendix D. In the following, the approximation error is estimated as the average of 10 measurements with 1000 random samples each. The results are presented in Figure 10.

The first column addresses the performance of the iterative Chebyshev approximation for the two multivariate Gaussian functions with respect to their dimension, in both the serial and interleaved qubit orders. As suggested by Figures 10(a) and 10(b), the accuracy and complexity of the method now largely depends on the qubit order. The product Gaussian distribution (30) is stably loaded in the serial order with a reduced bond dimension, but has an exponentially growing bond dimension in the interleaved order as $e^{1.57m} \approx 5^m$, preventing any approximation beyond $m = 4$. On the other hand, the squeezed Gaussian distribution (31) is loaded efficiently in both the serial and interleaved orders, although more stably and accurately in the latter, exhibiting a sublinear bond dimension growth of $\mathcal{O}(m^{0.49})$ and implying an exponential advantage over its tensor counterpart. In all cases, the approximation error seems to be largely correlated to the bond dimension. Figure 10(c) shows that the CPU time scales polynomially cases except for the Gaussian with exponentially growing bond dimension. Interestingly, the squeezed function in interleaved order shows a superior performance than in serial order. This is in part due to its enhanced stability, which allows for a more aggressive simplification of the initial condition.

The second column addresses the parametrization of the results with the local truncation error induced by the tolerance ϵ , for the most stringent parameter setting of $n = 20$ and $m = 10$. The inefficient interleaved product Gaussian function is omitted. Figures 10(d) and 10(e) show how the tolerance parameterizes the error and maximum bond dimension similarly than in the univariate scenario. However, now the stability of the maximum bond dimension is enhanced in the interleaved qubit order. Figure 10(f) shows how this parameterization re-

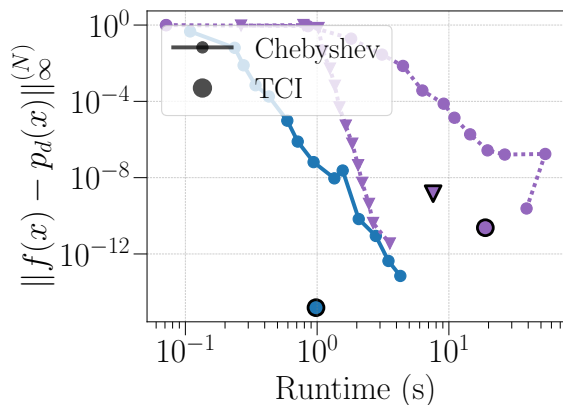


FIG. 11: CPU time required to reach a given approximation error for the MPS/QTT Chebyshev approximation method and TCI. The results for the Chebyshev approximation are parameterized with the tolerance ϵ between 10^{-1} and 10^{-14} . The large isolated markers correspond to TCI results, while the curves correspond to Chebyshev results. The functions are labeled following the legend of Figure 10(a), which is omitted for conciseness.

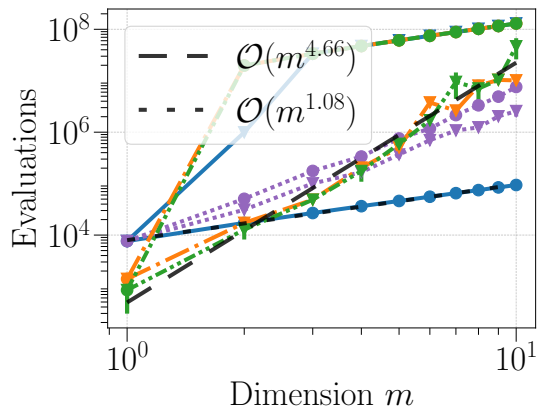


FIG. 12: Number of evaluations required by TCI for the four multivariate functions with respect to their dimension. The functions are labeled according to the legend shown in Figure 10(a), which is omitted for conciseness.

while still achieving values that are useful in practice, below 10^{-6} in all remaining cases.

Moreover, multivariate MPS Chebyshev approximations require many orders of magnitude less function evaluations than TCI. This is illustrated in Figure 12, showing that the amount of function evaluations required by TCI reaches several million, while Chebyshev approximations require of the order of $\mathcal{O}(d_{\max})$ evaluations. These results suggest that, as opposed to MPS Chebyshev approximations, TCI may be less suitable for scenarios where the function evaluations pose a significant overhead. A relevant example is given by the composition of

functions in generic states, for which function evaluation involves costly tensor contractions.

V. DISCUSSION

This work has explored the problem of loading univariate and multivariate functions in matrix product states or quantized tensor trains, motivated by their application in quantum-inspired numerical methods. To this end, an adaptation of the Chebyshev approximation algorithm has been proposed for MPS/QTT structures. This method is based on a non-linear algebraic framework for MPS/QTT polynomial addition and multiplication, which enables the translation of Chebyshev expansions and Clenshaw evaluation schemes.

The numerical studies illustrate that the Chebyshev MPS/QTT iterative algorithm is stable, achieves the theoretical convergence rates and requires polynomial resources both in time and memory. In particular, in the univariate case the method scales linearly with the interpolation order and sublinearly with the number of qubits. This scaling generalizes to multivariate functions, which also can be encoded using polynomial resources.

Furthermore, MPS Chebyshev approximations provide a generic framework for function composition on MPS/QTT that enables non-linear manipulation of generic states. These capabilities are useful for the solution of non-linear equations with quantum-inspired methods [30] and the implementation of filters in Hamiltonian problems [31].

The following caveats are identified. First, the method is limited to the composition of low-dimensional, highly-differentiable functions, as the volume of the tensor of Chebyshev coefficients (19) scales exponentially with dimension. Second, the method generally exhibits slower convergence rates than multiscale interpolative constructions—requiring an interpolation order twice as large—and TCI. Finally, the required intermediate simplifications and linear combinations may be susceptible to numerical instabilities for large enough states.

Lastly, the following extensions are considered. On the one hand, the iterative scheme proposed for MPS Chebyshev expansions may be applicable for more elaborate algebraic schemes, such as rational approximation. These schemes may be able to extend the domain of applicability to piecewise smooth functions [47]. On the other hand, the exploration of function composition on irregular discretizations would be of interest as it enables efficient integration strategies, such as those based on Clenshaw-Curtis [48] or Gauss-Kronrod [49] quadrature rules.

The algorithms and methods shown in this work are freely available in the SeeMPS library [50], an open-source Python framework that aims to ease the prototyping and experimentation with MPS/QTT quantum-inspired algorithms. This library has supported other related applications [9, 16]. All the simulations described

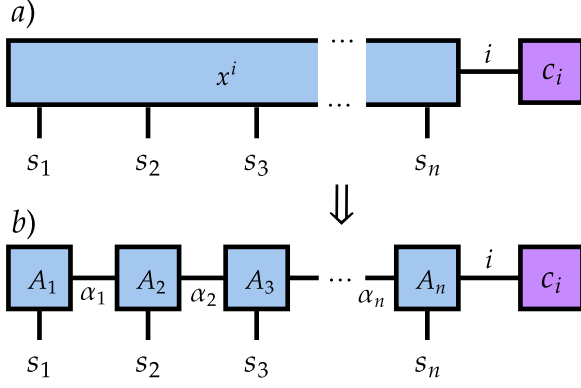


FIG. 13: Decomposition of a parametrized collection of monomials x^i contracted with a vector of coefficients c_i in a MPS.

in this study were conducted on a workstation equipped with an 18-core Intel(R) Xeon(R) W-2295 CPU and 64GB of RAM. The source files required to replicate the simulations are accessible in the public repository [51].

ACKNOWLEDGMENTS

This work has been supported by Spanish Projects No. PID2021-127968NB-I00 and No. PDC2022-133486-I00, funded by MCIN/AEI/10.13039/501100011033 and by the European Union “NextGenerationEU”/PRTR” 1. The authors acknowledge the discussions on related topics with A. Bou Comas and E. Staffetti. The authors also gratefully acknowledge the Scientific Computing Area (AIC), SGAI-CSIC, for their assistance while using the DRAGO Supercomputer for performing the simulations, and Centro de Supercomputaci3n de Galicia (CESGA) who provided access to the supercomputer FinisTerae. The authors thank the Institut Henri Poincar3 (UAR 839 CNRS-Sorbonne Universit3) and the LabEx CARMIN (ANR-10-LABX-59-01) for their support. PGM acknowledges the funds given by “FSE invierte en tu futuro” through an FPU Grant FPU19/03590 and by MCIN/AEI/10.13039/501100011033.

Appendix A: Analytical encoding of polynomials in MPS/QTT

This Appendix provides a recipe to construct the MPS/QTT representation of the polynomials $f_d(x)$ of degree d

$$f_d(x) = \sum_{i=0}^d p_i x^i \quad (\text{A1})$$

over a finite domain $x \in [a, b]$. The constructive proof creates a tensor representation for the discretization of

f on a grid of arbitrary density, with tensors $A_{i,r}^s \in \mathbb{C}^{\ell \times (d+1)^2}$ whose index sizes are determined by polynomial degree $\chi = d + 1$ and the quantization ℓ ($\ell = 2$ in our simulations).

The proof is done by induction. Starting from $|x_n^i\rangle$, the tensor decomposition of a monomial x^i over a grid with ℓ^n components, the construct derives a recipe for $|x_{n+1}^i\rangle$ by adding one more variable:

$$|x_{n+1}^i\rangle = \sum_{r=0}^d A_{r,i}^{s_{n+1}} |x_n^r\rangle |s_{n+1}\rangle. \quad (\text{A2})$$

The new discretization can be expressed in terms of the original, coarser-grained one $x(s_1, s_2, \dots, s_n)$ and a displacement that depends on the new quantization variable $s_{n+1} \in \{0, 1, \dots, \ell - 1\}$

$$x(\mathbf{s}_{n+1}) = x(\mathbf{s}_n) + \frac{d}{\ell^{n+1}} s_{n+1}. \quad (\text{A3})$$

Hence, it follows

$$x(\mathbf{s}_{n+1})^i = \sum_{r=0}^i x(\mathbf{s}_n)^r \left(\frac{s_{n+1}}{\ell^{n+1}}\right)^{i-r} \binom{i}{r} \quad (\text{A4})$$

$$= \sum_{r=0}^d x(\mathbf{s}_n)^r \left(\frac{s_{n+1}}{\ell^{n+1}}\right)^{i-r} \binom{i}{r} \Theta(i-r) \quad (\text{A5})$$

$$=: \sum_{r=0}^d x(\mathbf{s}_n)^r A_{r,i}^{s_{n+1}}. \quad (\text{A6})$$

This expression uses the asymmetric Heaviside function, which is nonzero $\Theta(i-r) = 1$ only when $i \geq r$.

Equation (A6) is a recursive formula to construct the tensor representation of $|x_n^i\rangle$

$$|x_n^i\rangle = A_{0,\alpha_1}^{s_1} A_{\alpha_1,\alpha_2}^{s_2} \cdots A_{\alpha_{n-1},i}^{s_n} |s_1, s_2, \dots, s_n\rangle, \quad (\text{A7})$$

with tensors

$$A_{r,k}^{s_n} = \left(\frac{s_n}{\ell^n}\right)^{k-r} \binom{k}{r} \Theta(k-r), \quad (\text{A8})$$

where the indices r, k, α_j run between 0 and d . This construct is a tensor network with one free index, which is the degree of the monomial, as illustrated in Fig. 13a.

A similar proof allows building a reversed construct

$$|x_n^i\rangle = B_{i,\alpha_1}^{s_1} B_{\alpha_1,\alpha_2}^{s_2} \cdots B_{\alpha_{n-1},i}^{s_n} |s_1, s_2, \dots, s_n\rangle, \quad (\text{A9})$$

with flipped tensors

$$B_{k,r}^{s_n} = \left(\frac{s_n}{\ell^n}\right)^{k-r} \binom{k}{r} \Theta(k-r). \quad (\text{A10})$$

The interest of these constructs is that they extend to arbitrary polynomials of a fixed degree. Thus, for any combination of monomials of degree d or lower we acquire a tensor network decomposition with bonds of size $d + 1$

$$p(x) = \sum_i c_i x^i \Rightarrow |p(x)_n\rangle = \sum_i c_i |x_n^i\rangle, \quad (\text{A11})$$

from either Eq. (A7) or (A9). This construct only modifies one of the tensors in the expansion [c.f. Fig. 13b].

Appendix B: Performance of the Clenshaw evaluation method

This Appendix compares the two possible ways to evaluate the partial sums (12) and (17) for MPS/QTT Chebyshev approximation. The former is based on evaluating the Chebyshev polynomials $T_k(g)$ using the recurrence relation (25) and then directly evaluating the partial sums. The latter is based on the Clenshaw summation method, based on evaluating (23).

In most occasions, both evaluation methods have similar accuracy, but the Clenshaw method is more efficient, with smaller runtimes and maximum bond dimensions, provided the expansion uses the right number of polynomials. If the expansion goes beyond the required order, introducing contributions whose weight is below machine precision, the algorithm will lead to an unbounded growth of the intermediate bond dimensions, resulting in a significantly longer runtime. However, since the optimal order can be estimated beforehand through the decay of the Chebyshev coefficients, this should not pose a practical problem.

A suitable benchmark to compare both evaluation orders is the Chebyshev expansion of the oscillating function (27), using the most stringent parameters $n = 25$, $d = 1300$ and $\epsilon = 10^{-14}$. Figure 14 shows how the Clenshaw method leads to significantly smaller maximum bond dimension and runtimes. Similar accuracies between both methods are noted and omitted for conciseness.

Figure 15, shows the maximum bond dimension of the intermediate steps, $\chi_{i, \max}$, for the interpolation of the Gaussian function (26) up to an order $d = 200$. The Clenshaw method overestimates the intermediate bond dimensions when the interpolation order is also overestimated—i.e., the expansion included terms with a contribution below machine precision—. Interestingly, the direct evaluation does not exhibit this problem, which in this case would imply a better performance. However, this advantage ceases to exist when the required expansion order is properly estimated beforehand.

Appendix C: Tensor cross-interpolation

Tensor cross-interpolation (TCI), also known as “TT-cross”, is a well-known algorithm that computes the tensor-train representation of a black-box multivariate function from the sampling of its elements along specific patterns known as crosses. This function can implicitly represent a tensor, so TCI specializes as an efficient tensor decomposition method. Other potential applications of TCI include function composition and loading functions in MPO structures.

TCI exhibits a polynomial time complexity and offers an exponential advantage over the standard tensor decomposition method based on iterated SVD. This establishes it as one of the preferred method for loading

highly multivariate functions. It has demonstrated a remarkable performance in multivariate integration [20, 39, 52, 53], with applications in quantum field theory [20] and condensed matter physics [42, 54], showing exponential improvements over state-of-the-art integration techniques [39, 53]. Moreover, it has proven useful for other tasks including multivariate optimization [55, 56], multivariate distribution sampling [57] or quantum state tomography [58].

TCI was introduced in a seminal work by Oseledets [23] and conceived as a generalization of a low-rank matrix decomposition, known as the skeleton decomposition [59], to tensors. This early version of TCI, however, was not rank adaptive and required prior knowledge of the tensor ranks. Since its introduction, numerous advancements have been made to improve the efficiency and rank adaptivity of TCI. One such advancement is the incorporation of two-site optimizations, similar to those used in the Density Matrix Renormalization Group (DMRG) algorithm [40]. Other approaches have introduced greedy optimization strategies that involve the use of “pivots” [20, 39, 41]. Additionally, rank-adaptive one-site optimizations utilizing the rectangular skeleton decomposition [60] have been proposed.

The implementation of TCI used in this work follows this latter method, and is based on a former tensor-train implementation employed in Refs. [55, 61].

1. The skeleton decomposition

The skeleton decomposition is a low-rank matrix decomposition of a matrix A in a column submatrix C , a row submatrix R and a submatrix \hat{A} formed by the intersection of the chosen columns and rows, as

$$A = C\hat{A}^{-1}R. \quad (\text{C1})$$

This decomposition is exact for rank- r matrices if r linearly independent rows and columns are chosen. In the approximate case, its accuracy is dependent on the chosen set of rows and columns. A notation that includes the sets of indices explicitly is adopted for convenience. Given the sets $\mathcal{I} = \{i_1, \dots, i_r\}$ and $\mathcal{J} = \{j_1, \dots, j_r\}$, each containing r indices for rows and columns respectively, the skeleton decomposition can be reformulated as

$$A = A(\mathbb{I}, \mathcal{J}) [A(\mathcal{I}, \mathcal{J})]^{-1} A(\mathcal{I}, \mathbb{J}), \quad (\text{C2})$$

as depicted in Figure 16. Here, \mathbb{I} and \mathbb{J} are the sets of all rows and columns of A .

Finding the optimal set of r rows and columns for the skeleton decomposition is challenging [62]. However, there are effective heuristics for achieving a good approximation [59]. These heuristics follow the “maxvol principle”, which suggests that an accurate approximation is achieved by maximizing the “volume”—defined as the

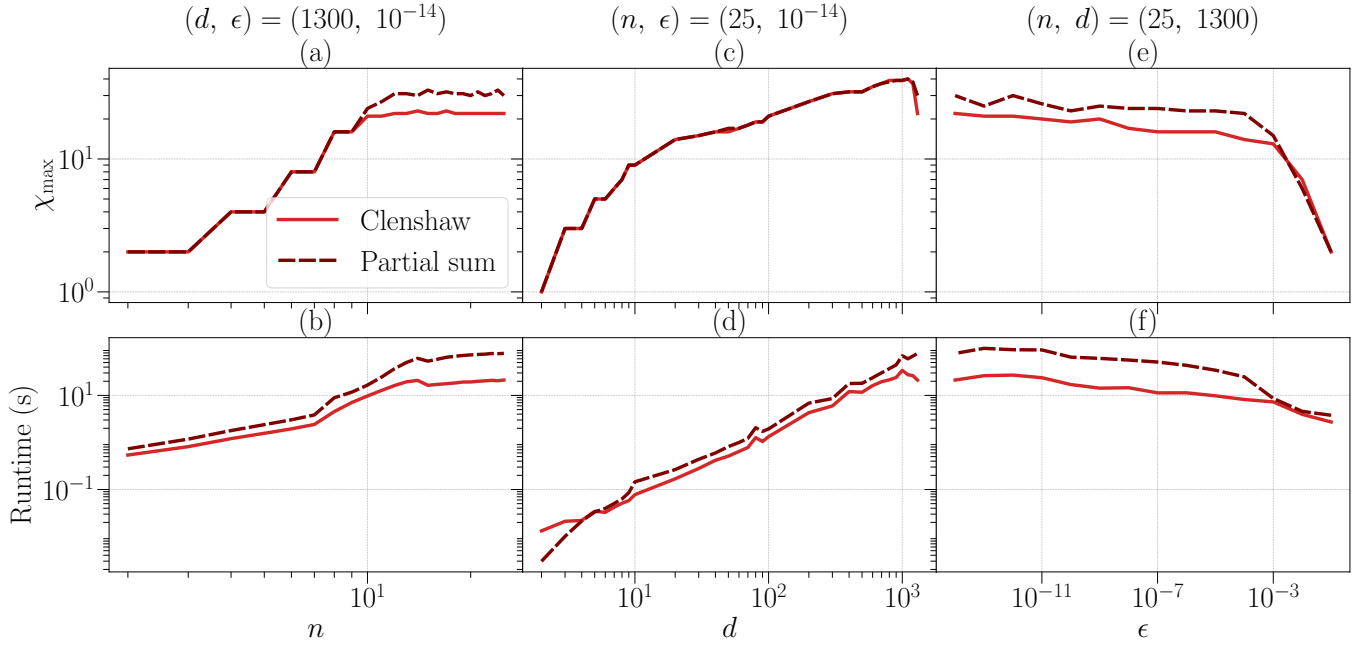


FIG. 14: Comparison between the Clenshaw evaluation (23) (in red) and the direct evaluation (in brown) of the partial sum (24) for the MPS Chebyshev approximation of the oscillating function (27). This study follows the same structure as the numerical studies performed in Section IV, showing individual experiments with mutually shared axes in logarithmic scale.

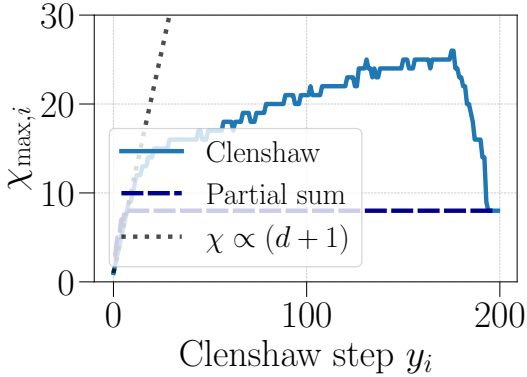


FIG. 15: Maximum bond dimension for the d intermediate states of a MPS approximation for the Gaussian (26) with $n = 25$, $d = 200$ and $\epsilon = 10^{-14}$. The dotted line represents the polynomial bound $\chi \propto d + 1$.

absolute value of the determinant—of the intersection submatrix \hat{A} , as

$$\text{vol}(\hat{A}) := |\det \hat{A}|. \quad (\text{C3})$$

This principle is generalizable to cases where the intersection submatrices are rectangular, allowing for the selection of rectangular submatrices of maximum volume [60].

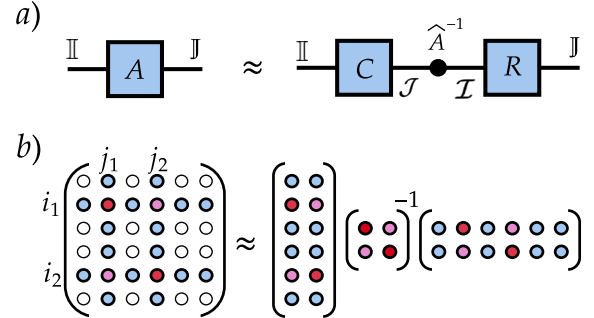


FIG. 16: Skeleton decomposition of the matrix A , using tensor network notation (a) and explicitly showing the matrix elements (b). The selected rows and columns (blue) are contained in the index sets \mathcal{I} and \mathcal{J} , resulting in intersections (pink) and pivots (red).

2. Generalization to tensors

The skeleton decomposition can be applied on the “unfolding” matrices of a tensor. These matrices are given by the reorganization of the tensor’s indices in two distinct multi-indices. Given a tensor $A(s_1, s_2, \dots, s_n)$, where each index s_j has a corresponding size \mathbb{I}_k , its indices before and after any chosen position k can be grouped into

two multi-indices,

$$\begin{aligned} s_{<k} &:= s_1 s_2 \dots s_{k-1} \in \mathbb{I}_1 \times \mathbb{I}_2 \times \dots \times \mathbb{I}_{k-1}, \\ s_{>k} &:= s_{k+1} s_{k+2} \dots s_n \in \mathbb{I}_{k+1} \times \mathbb{I}_{k+2} \times \dots \times \mathbb{I}_n. \end{aligned} \quad (\text{C4})$$

Then, by grouping the index s_k with the multi-index $s_{<k}$, it can be unfolded in a matrix

$$A(s_1, s_2, \dots, s_n) := A(s_{<k} s_k, s_{>k}). \quad (\text{C5})$$

The skeleton decomposition of this matrix computes the sets multi-indices $\mathcal{I}_{\leq k}$ and $\mathcal{J}_{>k}$, that are respectively in $s_{<k} s_k$ and $s_{>k}$, which maximize the volume of the intersection matrix:

$$\begin{aligned} A(s_{<k} s_k, s_{>k}) &\approx \\ &\approx A(s_{<k} s_k, \mathcal{J}_{>k}) [A(\mathcal{I}_{\leq k}, \mathcal{J}_{>k})]^{-1} A(\mathcal{I}_{\leq k}, s_{>k}). \end{aligned} \quad (\text{C6})$$

The tensor-train decomposition of the tensor A is achieved by sequentially applying the skeleton decomposition to each of its unfolding matrices. Initially, the decomposition targets the matrix formed by the multi-indices $\mathcal{I}_{\leq 1}$ and $\mathcal{J}_{>1}$, calculating a matrix $A(s_{<1} s_1, \mathcal{J}_{>1}) [A(\mathcal{I}_{\leq 1}, \mathcal{J}_{>1})]^{-1}$ which is then unfolded to represent the first tensor of the tensor-train. The subsequent structure, represented by $A(\mathcal{I}_{\leq 1}, s_{>1})$, is then unfolded into a matrix $A(\mathcal{I}_{\leq 1} s_2, s_{>2})$ by combining the index s_2 with the set $\mathcal{I}_{\leq 1}$, and then similarly decomposed. This process is sequentially applied across all unfolding matrices of A , systematically constructing the tensor-train

$$\begin{aligned} &A(s_1, s_2, \dots, s_n) \approx \\ &\approx A(s_1, \mathcal{J}_{>1}) [A(\mathcal{I}_{<2}, \mathcal{J}_{>1})]^{-1} \times \\ &\times A(\mathcal{I}_{<2}, s_2, \mathcal{J}_{>2}) [A(\mathcal{I}_{<3}, \mathcal{J}_{>2})]^{-1} \times \dots \\ &\dots \times A(\mathcal{I}_{<k}, s_k, \mathcal{J}_{>k}) [A(\mathcal{I}_{<k+1}, \mathcal{J}_{>k})]^{-1} \times \dots \\ &\dots \times A(\mathcal{I}_{<n}, s_n). \end{aligned} \quad (\text{C7})$$

The elements $A(\mathcal{I}_{<k}, s_k, \mathcal{J}_{>k})$ are referred to as “fibers”. These fibers become transform into the cores of the tensor train following their contraction with the inverse intersection matrices $[A(\mathcal{I}_{<k+1}, \mathcal{J}_{>k})]^{-1}$. By construction, the multi-indices $\mathcal{I}_{<k}$ and $\mathcal{J}_{>k}$ are nested, satisfying the properties

$$\mathcal{I}_{k+1} \subset \mathcal{I}_k \times s_k \quad \text{and} \quad \mathcal{J}_k \subset s_{k+1} \times \mathcal{J}_{k+1}. \quad (\text{C8})$$

In that case, the tensor-train approximation preserves the elements of A that are included in the fibers, while it interpolates the remaining elements [39].

This approach is inefficient, as it acts on the explicit tensor representation of A . In practice, TCI provides an exponential improvement by acting on a black-box representation of A . It begins with an initial tensor-train approximation of rank- r , as in (C7), that includes a collection of nested multi-indices \mathcal{J}_k . Then, it starts a recursive procedure. The first fiber of the approximation, $A(s_1, \mathcal{J}_{>1})$, is sampled from the black-box function and decomposed. This produces a set of multi-indices $\mathcal{I}_{<2}$, which facilitates the sampling of the intersection submatrix $A(\mathcal{I}_{<2}, \mathcal{J}_{>1})$ and the subsequent fiber

$A(\mathcal{I}_{<2}, s_2, \mathcal{J}_{>2})$. This process is recursively continued through the final tensor of the approximation, after which the procedure reverses from the last tensor back to the first. Each of these “sweeps” updates every tensor core of the approximation, repeating in a left-to-right and right-to-left iterative scheme until a convergence criterion is satisfied.

This formulation is not rank-adaptive, as it does not adjust the tensor ranks dynamically. This limitation can be addressed by replacing the standard skeleton decomposition with its generalization for rectangular matrices [60]. This allows for the progressive expansion of the index sets $\mathcal{I}_{<k}$ and $\mathcal{J}_{>k}$, increasing the ranks or bond dimensions of the approximation following each sweep. This avoids the need to estimate the ranks of the solution in advance, and allows to start with a rank-1 approximation which can be taken at random. The expansion rate of the index sets is controlled by a hyperparameter. In this work, it is set to perform a rank-1 increase at every decomposition, hence increasing the ranks by two at every complete sweep.

3. Extension to MPS/QTT

TCI can be extended to compute MPS/QTT structures by imposing the quantization of the degrees of freedom of the black-box function. This involves sampling a different set of fibers $A(\mathcal{I}_{<k}, s_k, \mathcal{J}_{>k})$ from the sets of MPS/QTT indices. In turn, these indices are related to the tensor-train indices—that is, the indices labeling the discretization nodes of the function degrees of freedom—by a simple linear map which arises naturally from the k -nary representation shown in Eq. (3). This map depends on the order of the MPS tensors, as well as on the number of tensors assigned to each dimension. Instead of deriving a general expression, we illustrate this map for a simple example. Consider a bivariate function $f(x_1, x_2)$ with n_1 and n_2 qubits per dimension. This function yields the linear maps

$$M_{ij}^{\text{serial}} = \begin{pmatrix} 2^{n_1-1} & 0 \\ 2^{n_1-2} & 0 \\ \vdots & \vdots \\ 2^0 & 0 \\ 0 & 2^{n_2-1} \\ 0 & 2^{n_2-2} \\ \vdots & \vdots \end{pmatrix}, \quad M_{ij}^{\text{intl}} = \begin{pmatrix} 2^{n_1-1} & 0 \\ 0 & 2^{n_2-1} \\ 2^{n_1-2} & 0 \\ 0 & 2^{n_2-2} \\ \vdots & \vdots \end{pmatrix} \quad (\text{C9})$$

for the serial and interleaved orders respectively. These maps facilitate the identification and computation of the appropriate fibers for MPS/QTT decomposition, independent of the specific details of the underlying TCI implementation.

Crucially, often the pivot matrices $A(\mathcal{I}_{<k+1}, \mathcal{J}_{>k})$ of MPS/QTT structures are ill-conditioned for inversion, leading to significant numerical instabilities. This can be

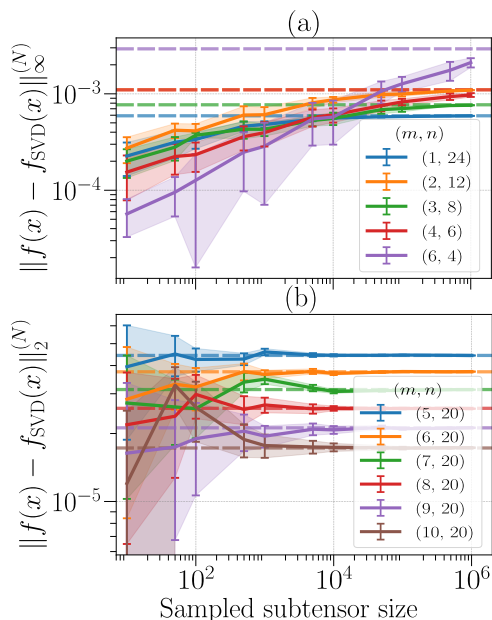


FIG. 17: (a) Error analysis between a product Gaussian distribution and its SVD approximation. Comparison between the error in L^∞ norm of the full discretization tensor and of randomly sampled subtensors. (b) Error analysis between a larger product Gaussian distribution computed with SVD and with iterated Chebyshev expansions. Comparison between the error in norm-2 calculated using the scalar product and using samples. The legends represent the configurations (m, n) of dimension m and qubits per dimension n . The error bars represent the standard deviation for 100 iterations.

avoided by orthogonalizing the fibers prior to performing the skeleton decomposition using the QR decomposition, enhancing the stability and accuracy of the method [23].

Appendix D: Evaluation of the MPS/QTTE error estimation using random sampling

Evaluating the distance in norm L^p of a multivariate function with its approximation requires assessing their exponentially large discretization tensors. However, it can be estimated following a Monte Carlo approach from a collection of random samples. This Appendix assesses this estimation for the product Gaussian distribution up to 200 qubits in two experiments.

The first experiment, shown in Figure 17(a), consists in loading the product Gaussian function 30 using SVD with a tolerance of $\epsilon = 10^{-8}$, from 1 to 6 dimensions and up to 24 qubits. Then, its error in L^∞ norm is estimated from a collection of random samples. Apparently, the estimation converges monotonically to the error of the full discretization tensor with the number of samples.

The second experiment, shown in Figure 17(b) consists in loading the product Gaussian function with two different methods, up to 200 qubits, and comparing their error. The first method is given by the tensorization of the univariate function loaded with SVD. The second method is given by an iterative MPS Chebyshev expansion, following Section III. Then, the sampled error in L^2 norm is compared with the error computed as the MPS norm of their difference, given by their scalar product. Apparently, the sampled errors converge to the quasi-exact errors in L^2 norm given by their scalar product for more than 10^4 samples.

-
- [1] R. Orús, *Annals of Physics* **349**, 117 (2014).
 - [2] I. Affleck, T. Kennedy, E. H. Lieb, and H. Tasaki, *Phys. Rev. Lett.* **59**, 799 (1987).
 - [3] M. Fannes, B. Nachtergaele, and R. F. Werner, *Europhysics Letters* **10**, 633 (1989).
 - [4] S. Östlund and S. Rommer, *Phys. Rev. Lett.* **75**, 3537 (1995).
 - [5] J. Dukelsky, M. A. Martín-Delgado, T. Nishino, and G. Sierra, *Europhysics Letters* **43**, 457 (1998).
 - [6] S. R. White, *Physical Review Letters* **69**, 2863 (1992).
 - [7] I. V. Oseledets, *SIAM Journal on Scientific Computing* **33**, 2295 (2011).
 - [8] B. N. Khoromskij, *Constructive Approximation* **34**, 257 (2011).
 - [9] J. J. García-Ripoll, *Quantum* **5**, 431 (2021), arxiv:1909.06619 [quant-ph].
 - [10] S. V. Dolgov, B. N. Khoromskij, and I. V. Oseledets, *SIAM Journal on Scientific Computing* **34**, A3016 (2012).
 - [11] J. Chen, E. Stoudenmire, and S. R. White, *PRX Quantum* **4**, 040318 (2023).
 - [12] P. García-Molina, J. Rodríguez-Mediavilla, and J. J. García-Ripoll, *Physical Review A* **105**, 012433 (2022), arxiv:2104.02668 [quant-ph].
 - [13] L. Lin and S. R. White, *A Novel Method of Function Extrapolation Inspired by Techniques in Low-entangled Many-body Physics* (2023), arxiv:2308.09001 [quant-ph].
 - [14] S. Dolgov, B. Khoromskij, and D. Savostyanov, *Journal of Fourier Analysis and Applications* **18**, 915 (2012).
 - [15] N. Gourianov, M. Lubasch, S. Dolgov, Q. Y. van den Berg, H. Babae, P. Givi, M. Kiffner, and D. Jaksch, *Nature Computational Science* **2**, 30 (2022), arxiv:2106.05782 [physics, physics:quant-ph].
 - [16] P. García-Molina, L. Tagliacozzo, and J. J. García-Ripoll, *Global optimization of MPS in quantum-inspired numerical analysis* (2023), arxiv:2303.09430 [quant-ph].
 - [17] E. Ye and N. Loureiro, *Quantized tensor networks for solving the Vlasov-Maxwell equations* (2024), arxiv:2311.07756 [physics, physics:quant-ph].
 - [18] B. Khoromskij and A. Veit, *Computational Methods in Applied Mathematics* **16**, 145 (2016).
 - [19] R. Peng, J. Gray, and G. K.-L. Chan, *Physical Review Research* **5**, 013156 (2023).
 - [20] Y. Núñez Fernández, M. Jeannin, P. T. Dumitrescu, T. Kloss, J. Kaye, O. Parcollet, and X. Waintal, *Physical*

- Review X **12**, 041018 (2022).
- [21] C. Schön, E. Solano, F. Verstraete, J. I. Cirac, and M. M. Wolf, *Phys. Rev. Lett.* **95**, 110503 (2005).
- [22] A. A. Melnikov, A. A. Termanova, S. V. Dolgov, F. Neukart, and M. R. Perelshtein, *Quantum Science and Technology* **8**, 035027 (2023).
- [23] I. Oseledets and E. Tyrtyshnikov, *Linear Algebra and its Applications* **432**, 70 (2010).
- [24] Y. Hur, J. G. Hoskins, M. Lindsey, E. Stoudenmire, and Y. Khoo, *Applied and Computational Harmonic Analysis* **67**, 101575 (2023).
- [25] M. Lindsey, Multiscale interpolative construction of quantized tensor trains (2023), arxiv:2311.12554 [cs, math].
- [26] J. Chen and M. Lindsey, Direct interpolative construction of the discrete Fourier transform as a matrix product operator (2024), arXiv:2404.03182 [quant-ph].
- [27] J. C. Mason and D. C. Handscomb, *Chebyshev Polynomials* (CRC Press, Boca Raton; London New York, 2003).
- [28] L. N. Trefethen, *Approximation Theory and Approximation Practice, Extended Edition* (Society for Industrial and Applied Mathematics, Philadelphia, PA, 2019).
- [29] M. C. Bañuls, D. A. Huse, and J. I. Cirac, *Phys. Rev. B* **101**, 144305 (2020).
- [30] M. Lubasch, P. Moinier, and D. Jaksch, *Journal of Computational Physics* **372**, 587 (2018).
- [31] Y. Yang, S. Iblisdir, J. I. Cirac, and M. C. Bañuls, *Phys. Rev. Lett.* **124**, 100602 (2020).
- [32] J. I. Cirac, D. Pérez-García, N. Schuch, and F. Verstraete, *Rev. Mod. Phys.* **93**, 045003 (2021).
- [33] S. Iblisdir, J. I. Latorre, and R. Orús, *Phys. Rev. Lett.* **98**, 060402 (2007).
- [34] A. Gorodetsky, S. Karaman, and Y. Marzouk, *Computer methods in applied mechanics and engineering* **347**, 59 (2019).
- [35] S. V. Dolgov, B. N. Khoromskij, and I. V. Oseledets, *SIAM Journal on Scientific Computing* **34**, A3016 (2012), <https://doi.org/10.1137/120864210>.
- [36] J. I. Latorre, Image compression and entanglement (2005), arXiv:quant-ph/0510031 [quant-ph].
- [37] T. Shi and A. Townsend, *SIAM Journal on Matrix Analysis and Applications* **42**, 275 (2021).
- [38] B. Jobst, K. Shen, C. A. Riofrío, E. Shishenina, and F. Pollmann, arXiv preprint arXiv:2311.07666 (2023).
- [39] S. Dolgov and D. Savostyanov, *Computer Physics Communications* **246**, 106869 (2020), arxiv:1903.11554 [math].
- [40] D. Savostyanov and I. Oseledets, in *The 2011 International Workshop on Multidimensional (nD) Systems* (IEEE, Poitiers, France, 2011) pp. 1–8.
- [41] D. V. Savostyanov, *Linear Algebra and its Applications* **458**, 217 (2014), arxiv:1305.1818 [math].
- [42] M. K. Ritter, Y. Núñez Fernández, M. Wallerberger, J. von Delft, H. Shinaoka, and X. Waintal, *Physical Review Letters* **132**, 056501 (2024).
- [43] I. V. Oseledets, *Constructive Approximation* **37**, 1 (2013).
- [44] J. P. Boyd, *Chebyshev & Fourier Spectral Methods*, edited by C. A. Brebbia, S. A. Orszag, J. Argyris, K.-J. Bathe, A. S. Cakmak, J. Connor, R. McCrory, C. S. Desai, K.-P. Holz, F. A. Leckie, G. Pinder, A. R. S. Ponter, J. H. Seinfeld, P. Silvester, P. Spanos, W. Wunderlich, and S. Yip, *Lecture Notes in Engineering*, Vol. 49 (Springer Berlin Heidelberg, Berlin, Heidelberg, 1989).
- [45] C. W. Clenshaw, *Mathematics of Computation* **9**, 118 (1955).
- [46] J. A. Grant, *The Mathematical Gazette* **54**, 96 (1970).
- [47] T. A. Driscoll and B. Fornberg, *Numerical Algorithms* **26**, 77 (2001).
- [48] J. Waldvogel, *BIT Numerical Mathematics* **46**, 195 (2006).
- [49] G. H. Golub and J. H. Welsch, *Mathematics of computation* **23**, 221 (1969).
- [50] J. J. García-Ripoll, Minimal matrix-product state algorithms library., <https://github.com/juanjosegarcia-ripoll/seemps2> (2024).
- [51] J. J. Rodríguez-Aldavero, Simulations for the figures in the paper., https://github.com/jjrodriguezaldavero/seemps_chebyshev_approximation (2024).
- [52] L. I. Vysotsky, A. V. Smirnov, and E. E. Tyrtyshnikov, *Lobachevskii Journal of Mathematics* **42**, 1608 (2021), arxiv:2103.12129 [hep-ph].
- [53] B. Alexandrov, G. Manzini, E. W. Skau, P. M. D. Truong, and R. G. Vuchov, *Mathematics* **11**, 534 (2023).
- [54] A. Erpenbeck, W.-T. Lin, T. Blommel, L. Zhang, S. Iskakov, L. Bernheimer, Y. Núñez-Fernández, G. Cohen, O. Parcollet, X. Waintal, and E. Gull, *Physical Review B* **107**, 245135 (2023), arxiv:2303.11199 [cond-mat].
- [55] A. Chertkov, G. Ryzhakov, G. Novikov, and I. Oseledets, Optimization of Functions Given in the Tensor Train Format (2022), arxiv:2209.14808 [cs, math].
- [56] K. Sozykin, A. Chertkov, R. Schutski, A.-H. Phan, A. S. Cichocki, and I. Oseledets, *Advances in Neural Information Processing Systems* **35**, 26052 (2022).
- [57] S. Dolgov, K. Anaya-Izquierdo, C. Fox, and R. Scheichl, *Statistics and Computing* **30**, 603 (2020).
- [58] A. Lidiak, C. Jameson, Z. Qin, G. Tang, M. B. Wakin, Z. Zhu, and Z. Gong, Quantum state tomography with tensor train cross approximation (2022), arXiv:2207.06397 [quant-ph].
- [59] S. A. Goreinov, I. V. Oseledets, D. V. Savostyanov, E. E. Tyrtyshnikov, and N. L. Zamarashkin, How to Find a Good Submatrix, in *Matrix Methods: Theory, Algorithms and Applications* (WORLD SCIENTIFIC, 2010) pp. 247–256.
- [60] A. Mikhalev and I. V. Oseledets, *Linear Algebra and its Applications* **538**, 187 (2018), arxiv:1502.07838 [cs, math].
- [61] A. Chertkov, G. Ryzhakov, and I. Oseledets, *SIAM Journal on Scientific Computing* **45**, A2101 (2023).
- [62] J. J. Bartholdi, *Operations Research Letters* **1**, 190 (1982).